Analytical Characterization of Coverage Regions for STAR-RIS-aided NOMA/OMA Communication Systems

Farshad Rostami Ghadi, F. Javier López-Martínez, *Senior Member*, *IEEE*, and Kai-Kit Wong, *Fellow*, *IEEE*

***Abstract*—We provide an analytical characterization of the coverage region of simultaneously transmitting and reflecting reconfigurable intelligent surface (STAR-RIS)-aided two-user downlink communication systems. The cases of orthogonal multiple access (OMA) and non-orthogonal multiple access (NOMA) are considered, under the energy-splitting (ES) protocol. Results confirm that the use of STAR-RISs is beneficial to extend the coverage region, and that the use of NOMA provides a better performance compared to the OMA counterpart. However, the effect of imperfect successive interference cancellation degrades the performance of NOMA and needs to be considered for a realistic analysis.**

***Index Terms*—Coverage region, reconfigurable intelligent surface, non-orthogonal multiple access, energy-splitting**

I. Introduction

Reconfigurable intelligent surfaces (RISs) have been recently introduced as promising approaches to enhance the performance of coverage and energy efficiency in sixth-generation (6G) wireless communications [1], [2]. Generally speaking, RISs are engineered structures equipped with a large number of low-cost passive reflecting elements, which can intelligently reconfigure the wireless propagation environment by adjusting the electromagnetic response of each reflecting element, and thus enable a smart radio environment (SRE). Compared to multi-antenna and relay communication systems, RISs do not require dedicated radio frequency (RF) chains, which reduces energy consumption and hardware costs [3].

One of the key limitations of RISs is related to the need of transmitters and receivers to be located on the same side of the RIS, i.e., within the same *half-space* of the SRE. To further extend the potential of RISs to the entire *full-space*, the concept of simultaneously transmitting and reflecting RISs (STAR-RISs) has been proposed [4]. The use of STAR-RIS enables a 360° coverage region of SREs, which implies that separate reflection and refraction passive beamforming can be designed for the different serving areas [5]–[9].

Given the appealing features of STAR-RIS, there has been a growing interest to combine these devices with non-orthogonal multiple access (NOMA) techniques [10], with a special focus on the two-user case [11]–[14] as a key building block in communication theory. With the aim of maximizing the sum rate, the authors in [10] analyzed the STAR-RIS-assisted NOMA under the mode-switching (MS) protocol. The outage probability and diversity gain analysis for STAR-RIS-aided NOMA system with perfect and imperfect successive interference cancellation (SIC) were studied in [11] and [12]. In addition, by assuming fading channel correlation, the authors in [13] derived the outage probability for a STAR-RIS-aided NOMA network. Moreover, a coverage range maximization problem over a STAR-RIS-assisted NOMA network under a quality of service (QoS) requirement for each user was formulated in [14]. While this latter work showed the benefits of NOMA over conventional OMA in terms of coverage range extension from an optimization perspective, the performance characterization in terms of the achievable average rates is challenging due to the involved analytical derivations required in this scenario – even for the two-user case. Thus, motivated by the importance of rigorously analyzing the coverage area in STAR-RIS, we derive analytical compact expressions for the coverage regions for both transmitting and reflecting users over a STAR-RIS-aided downlink NOMA/OMA, by exploiting the definition of coverage region provided in [15]. Numerical results show that the proposed analytical expressions are rather accurate, and confirm: (*i*) STAR-RIS can significantly enhance the system performance in terms of the coverage region for the NOMA scenario compared with the OMA scheme; (*ii*) the effect of imperfect successive interference cancellation (SIC) degrades the performance of NOMA and may even revert its benefits, so it needs to be considered for practical deployments.

The remainder of this paper is organized as follows: Section (II) describes the system model of interest, while section III provides the analysis of the coverage region. Numerical results and conclusion are provided in Sections IV and V, respectively.

II. System Model

We consider a STAR-RIS aided downlink NOMA as shown in Fig. 1, where a single-antenna base station (BS) serves two single-antenna mobile users (i.e., reflecting user u_{r} and transmitting user u_{t}) aided by a fixed STAR-RIS with N elements. We assume that the direct link between the BS and the reflecting user u_{r} is blocked due to obstacles, such as trees or buildings, and thus only reflecting links via the STAR-RIS are considered for the reflecting user u_{r}. In addition, the transmitting user u_{t} is located behind the STAR-RIS, thereby

This work was funded in part by Junta de Andalucía through grant EMERGIA20-00297, and in part by MCIN/AEI/10.13039/501100011033 through grant PID2020-118139RB-I00.

Farshad Rostami Ghadi and F. Javier López-Martínez are with the Communications and Signal Processing Lab, Telecommunication Research Institute (TELMA), Universidad de Málaga, Málaga, 29010, (Spain). F. Javier López-Martínez is also with the Dept. Signal Theory, Networking and Communications, University of Granada, 18071, Granada (Spain) (e-mail: farshad@ic.uma.es, fjlm@ugr.es).

Kai-Kit Wong is with the Department of Electronic and Electrical Engineering, University College London, London WC1E 6BT, United Kingdom and with Yonsei Frontier Lab, Yonsei University, Seoul, 03722, Korea.(e-mail: kai-kit.wong@ucl.ac.uk).

Digital Object Identifier 10.1109/XXX.2021.XXXXXXX

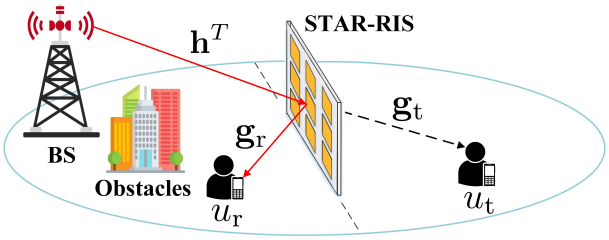

Fig. 1. System model of a downlink STAR-RIS-aided NOMA communication.

the direct link for the transmitting user u_t is blocked. Thus, the received signal at the user u_k, $\mathrm{k} \in \{\mathrm{r}, \mathrm{t}\}$ is expressed as

$$Y_\mathrm{t} = \sqrt{P}\mathbf{h}^T \mathbf{\Phi} \mathbf{g}_\mathrm{t} \left(\sqrt{p_\mathrm{t}} X_\mathrm{t} + \sqrt{p_\mathrm{r}} X_\mathrm{r}\right) + Z_\mathrm{t} \tag{1}$$

$$Y_\mathrm{r} = \sqrt{P}\mathbf{h}^T \mathbf{\Psi} \mathbf{g}_\mathrm{r} \left(\sqrt{p_\mathrm{t}} X_\mathrm{t} + \sqrt{p_\mathrm{r}} X_\mathrm{r}\right) + Z_\mathrm{r} \tag{2}$$

where P is the total transmit power, X_k denotes the symbol transmitted to user u_k with unit power (i.e., $\mathbb{E}\left[|X_\mathrm{k}|^2\right] = 1$), p_k is the power allocation factor for u_k, so that $p_t + p_r = 1$, and Z_k is the additive white Gaussian noise (AWGN) with zero mean and variance σ^2 at u_k. We consider the energy-splitting (ES)[1] protocol for our proposed STAR-RIS-aided network. Hence, we assume that all elements of the STAR-RIS simultaneously operate refraction and reflection modes, while the total radiation energy is split into two parts, i.e, $\mathbf{\Phi} = \mathrm{diag}\left(\left[\beta_{\mathrm{t},1}\mathrm{e}^{j\phi_1}, \beta_{\mathrm{t},2}\mathrm{e}^{j\phi_2}, ..., \beta_{\mathrm{t},N}\mathrm{e}^{j\phi_N}\right]\right)$ and $\mathbf{\Psi} = \mathrm{diag}\left(\left[\beta_{\mathrm{r},1}\mathrm{e}^{j\psi_1}, \beta_{\mathrm{r},2}\mathrm{e}^{j\psi_2}, ..., \beta_{\mathrm{r},N}\mathrm{e}^{j\psi_N}\right]\right)$ denote the STAR-RIS transmitting and reflecting coefficients matrices, respectively, where ϕ_n and ψ_n are the adjustable phases induced by the nth element of the STAR-RIS during transmission and reflection, whereas $\beta_{\mathrm{k},n}$ denote the adjustable transmission/reflection coefficients, with $\beta_{\mathrm{r},n}^2 + \beta_{\mathrm{t},n}^2 \leq 1$ due to the passive nature of the STAR-RIS. In order to minimize the system complexity, we assume in the sequel that all elements have the same amplitude coefficients [14], i.e., $\beta_{\mathrm{k},n} = \beta_\mathrm{k}, \forall n = 1 \ldots N$. The vectors $\mathbf{h}^T = d^{-\alpha}\left[h_1\mathrm{e}^{-j\theta_1}, h_2\mathrm{e}^{-j\theta_2}, ..., h_N\mathrm{e}^{-j\theta_N}\right]$, $\mathbf{g}_\mathrm{t} = d_\mathrm{t}^{-\alpha}\left[g_{\mathrm{t},1}\mathrm{e}^{-j\zeta_1}, g_{\mathrm{t},2}\mathrm{e}^{-j\zeta_2}, ..., g_{\mathrm{t},N}\mathrm{e}^{-j\zeta_N}\right]$, and $\mathbf{g}_\mathrm{r} = d_\mathrm{r}^{-\alpha}\left[g_{\mathrm{r},1}\mathrm{e}^{-j\eta_1}, g_{\mathrm{r},2}\mathrm{e}^{-j\eta_2}, ..., g_{\mathrm{r},N}\mathrm{e}^{-j\eta_N}\right]$ contain the channel coefficients from the BS to each element of the STAR-RIS, the channel coefficients from each element of the STAR-RIS to u_t, and the channel coefficients from each element of the STAR-RIS to u_r, respectively. The terms d, d_t, and d_r define the distances between the BS and the STAR-RIS, the distance between the STAR-RIS and u_t, and the distance between the STAR-RIS and u_r, respectively, where α is the path-loss exponent. In addition, h_n, $g_{\mathrm{t},n}$, and $g_{\mathrm{r},n}$ are the amplitudes of the corresponding channel coefficients, and $\mathrm{e}^{-j\theta_n}$, $\mathrm{e}^{-j\zeta_n}$, and $\mathrm{e}^{-j\eta_n}$ represent the phases of the respective links.

As per the principles of NOMA, the BS transmits the signals of both reflecting and transmitting users using the same time and frequency resources by superposition coding. Besides, the NOMA user with a better channel condition conducts SIC, while the other user decodes its signal directly treating interference as noise. Without loss of generality, we assume $d_\mathrm{r} < d_\mathrm{t}$ representing the scenario on which a STAR-RIS is deployed to overcome blockages for reflection users (see Fig. 1). For the sake of notational simplicity yet without loss of generality, we assume a fixed decoding order based on path loss [11], [12], [16], [17] so that the strong user u_r operates the SIC process. This implies in turn that the user in the transmission plane u_t is allocated more power by the BS (i.e., $p_\mathrm{r} < p_\mathrm{t}$). Thus, the signal-to-interference-plus-nois ratio (SINR) of the SIC process for u_r can be defined as

$$\gamma_\mathrm{sic} = \frac{\frac{\rho p_\mathrm{r} \beta_\mathrm{r}^2}{d^\alpha d_\mathrm{r}^\alpha}\left|\sum_{n=1}^N h_n g_{\mathrm{r},n}\mathrm{e}^{j(\phi_n-\theta_n-\zeta_n)}\right|^2}{\frac{\rho p_\mathrm{t} \beta_\mathrm{r}^2}{d^\alpha d_\mathrm{r}^\alpha}\left|\sum_{n=1}^N h_n g_{\mathrm{r},n}\mathrm{e}^{j(\phi_n-\theta_n-\zeta_n)}\right|^2 + 1}, \tag{3}$$

where $\rho = P/\sigma^2$ is the transmit signal-to-noise ratio (SNR). The effect of noise introduces some imperfections in the process of SIC, so that the message destined to u_t cannot be perfectly canceled by u_r and a residual error terms appears [18]. This can be modeled as a complex Gaussian random variable (RV) h_sic with zero mean and variance σ_sic^2, i.e., $h_\mathrm{sic} \sim \mathcal{CN}\left(0, \sigma_\mathrm{sic}^2\right)$. Hence, the overall SINR at u_r under imperfect SIC can be expressed as

$$\gamma_\mathrm{r}^{\mathcal{N}} = \frac{\rho d^{-\alpha} d_\mathrm{r}^{-\alpha} p_\mathrm{r} \beta_\mathrm{r}^2 \left|\sum_{n=1}^N h_n g_{\mathrm{r},n}\mathrm{e}^{j(\phi_n-\theta_n-\zeta_n)}\right|^2}{\rho\omega\left|h_\mathrm{sic}\right|^2 + 1}, \tag{4}$$

where $\omega \in (0, 1]$ is the controlling factor of imperfect SIC so that $\omega \to 0$ indicates the perfect SIC scenario as a special case. At the same time, u_t directly decodes its signal by considering the signal of u_r as interference. Thus, the SINR at u_t can be expressed as

$$\gamma_\mathrm{t}^{\mathcal{N}} = \frac{\rho p_\mathrm{t} \beta_\mathrm{t}^2 d^{-\alpha} d_\mathrm{t}^{-\alpha} \left|\sum_{n=1}^N h_n g_{\mathrm{t},n}\mathrm{e}^{j(\psi_n-\theta_n-\eta_n)}\right|^2}{\rho p_\mathrm{r} \beta_\mathrm{t}^2 d^{-\alpha} d_\mathrm{t}^{-\alpha} \left|\sum_{n=1}^N h_n g_{\mathrm{t},n}\mathrm{e}^{j(\psi_n-\theta_n-\eta_n)}\right|^2 + 1}. \tag{5}$$

On the other hand, the SNR at user u_k in OMA can be respectively defined as [19]

$$\gamma_\mathrm{r}^{\mathcal{O}} = \rho d^{-\alpha} d_\mathrm{r}^{-\alpha} \beta_\mathrm{r}^2 \left|\sum_{n=1}^N h_n g_{\mathrm{r},n}\mathrm{e}^{j(\phi_n-\theta_n-\zeta_n)}\right|^2, \tag{6}$$

$$\gamma_\mathrm{t}^{\mathcal{O}} = \rho d^{-\alpha} d_\mathrm{t}^{-\alpha} \beta_\mathrm{t}^2 \left|\sum_{n=1}^N h_n g_{\mathrm{t},n}\mathrm{e}^{j(\psi_n-\theta_n-\eta_n)}\right|^2. \tag{7}$$

Aiming to maximize the SNR at both reflecting and transmitting users, and as a benchmark for upper bounding the achievable performances, the ideal phase shifting is considered in the proposed system model [11]. Without loss of generality, we assume that all channels undergo Rayleigh fading. Even in this case, the equivalent channels at both users include a sum of products of RVs, which does not admit a tractable probability density function (PDF) expression. For this purpose, we exploit a Gamma approximation to derive equivalent channel distributions, which is reportedly more accurate than the central limit theorem (CLT) approximation [20]. Thus,

[1]These results can extended to the mode-switching (MS) and time-switching (TS) modes by allocating different numbers of active STAR-RIS elements or time blocks, respectively.

by defining $W_{\rm k} = \left|\sum_{n=1}^{N} h_n g_{{\rm k},n}\right|^2$, the PDF of $W_{\rm k}$ can be approximated as

$$f_{W_{\rm k}}\left(w_{\rm k}\right) = \frac{w_{\rm k}^{\kappa-1}{\rm e}^{-\frac{w_{\rm k}}{\tau}}}{\Gamma\left(\kappa\right)\tau^{\kappa}}, \tag{8}$$

where $\kappa = \frac{N\pi^2}{16-\pi^2}$ and $\tau = \frac{16-\pi^2}{4\pi}$ denote the shape and scale parameters, respectively.

III. Coverage Region Analysis

We now derive the analytical expressions of the coverage regions for both reflecting and transmitting users. To this end, we exploit the concept of coverage region provided in [15, Def. 2]. Without loss of generality, we assume that the BS is located at the origin of the two-dimensional coordinate and the STAR-RIS is placed at the fixed distance d from the BS. Under such an assumption, the coverage region can be defined as the geographic area for which the rates $R_{\rm r} > 0$ and $R_{\rm t} > 0$ are guaranteed, i.e.,

$$\mathcal{G}\left(d_{\rm t}, d_{\rm r}\right) \triangleq \left\{d_{\rm t}, d_{\rm r}, C_{\rm t}\left(d_{\rm t}\right) > R_{\rm t}, C_{\rm r}\left(d_{\rm r}\right) > R_{\rm r}\right\}, \tag{9}$$

where $C_{\rm t}\left(d_{\rm t}\right) = \mathbb{E}_{\gamma_{\rm t}}\left[\log_2\left(1+\gamma_{\rm t}\right)\right]$ and $C_{\rm r}\left(d_{\rm r}\right) = \mathbb{E}_{\gamma_{\rm r}}\left[\log_2\left(1+\gamma_{\rm r}\right)\right]$ denote the channel capacity when the users $u_{\rm t}$ and $u_{\rm t}$ are located at distances $d_{\rm t}$ and $d_{\rm r}$, respectively.

Remark 1. *The coverage region in* (9) *refers to the maximum distance $d_{\rm k}$ that user $u_{\rm k}$ can have from the STAR-RIS as far as reliable communication is guaranteed. This definition is related to an expectation over the achievable rate classically associated to an ergodic setting, which is also relevant in a block-fading setting with link adaptation capabilities [21].*

Theorem 1. *The coverage region over a STAR-RIS-aided NOMA communication for users $u_{\rm r}$ and $u_{\rm t}$ with defined parameters $R_{\rm k}^{\mathcal{N}}$, τ, κ, ρ, ω, and $\beta_{\rm k}$ is respectively given by*

$$R_{\rm r}^{\mathcal{N}} \leq \frac{{\rm E}_1\left(\frac{1}{\rho\omega\sigma_{\rm sic}^2}\right)}{{\rm e}^{-\frac{1}{\rho\omega\sigma_{\rm sic}^2}}\ln 2}\left[\rho\omega\left(1-\frac{\tau p_{\rm r}\beta_{\rm r}^2}{\omega d^{\alpha}d_{\rm r}^{\alpha}\sigma_{\rm sic}^2}\right)^{-\kappa}-1\right], \tag{10}$$

$$R_{\rm t}^{\mathcal{N}} \leq \frac{1}{\Gamma(\kappa)\ln 2}G_{3,2}^{1,3}\left(\frac{\tau\rho\beta_{\rm t}^2}{d^{\alpha}d_{\rm t}^{\alpha}}\,\middle|\,\begin{matrix}(1-\kappa,1,1)\\(1,0)\end{matrix}\right) - \frac{1}{\Gamma(\kappa)\ln 2}G_{3,2}^{1,3}\left(\frac{\tau\rho p_{\rm r}\beta_{\rm t}^2}{d^{\alpha}d_{\rm t}^{\alpha}}\,\middle|\,\begin{matrix}(1-\kappa,1,1)\\(1,0)\end{matrix}\right), \tag{11}$$

in which ${\rm E}_n(.)$ and $G_{p,q}^{m,n}(.)$ denote the generalized exponential integral function and Meijer's G-function, respectively.

Proof. The coverage region is expressed in terms of expectations over the random equivalent channel $w_{\rm k}$ and the RV $S = |h_{\rm sic}|^2$ such that $S \sim {\rm Exp}\left(\sigma_{\rm sic}^2\right)$. Thus, we first determine the coverage region of $u_{\rm r}$ as follows

$$R_{\rm r}^{\mathcal{N}} \leq \mathbb{E}_{w_{\rm r},s}\left[\log_2\left(1+\frac{\rho d^{-\alpha}d_{\rm r}^{-\alpha}p_{\rm r}\beta_{\rm r}^2 w_{\rm r}}{\rho\omega s+1}\right)\right] \tag{12}$$

$$= \mathbb{E}_{w_{\rm r},s}\left[\log_2\left(1+\rho\omega s+\frac{\rho p_{\rm r}\beta_{\rm r}^2 w_{\rm r}}{d^{\alpha}d_{\rm r}^{\alpha}}\right)\right] - \mathbb{E}_s\left[\log_2\left(1+\rho\omega s\right)\right] \tag{13}$$

$$= \int_0^{\infty}\log_2\left(1+t\right)f_T(t)dt - \int_0^{\infty}\log_2\left(1+\rho\omega s\right)f_S(s)ds, \tag{14}$$

where $f_T(t)$ and $f_S(s)$ are the PDF of the RVs $T = \rho\omega S + \frac{\rho p_{\rm r}\beta_{\rm r}^2}{d^{\alpha}d_{\rm r}^{\alpha}}W_{\rm r}$ and S, respectively. Since S follows the exponential distribution, its PDF can be given by $f_S(s) = \frac{1}{\sigma_{\rm sic}^2}{\rm e}^{-\frac{s}{\sigma_{\rm sic}^2}}$. In addition, by considering $f_{W_{\rm r}}\left(w_{\rm r}\right)$ from (8) and $f_S(s)$, the PDF of T can be determined after some mathematical manipulations as follows

$$f_T(t) = \frac{\left(\frac{1}{\tau}-\frac{p_{\rm r}\beta_{\rm r}^2}{\omega d^{\alpha}d_{\rm r}^{\alpha}\sigma_{\rm sic}^2}\right)^{-\kappa}}{\tau^{\kappa}\sigma_{\rm sic}^2}\exp\left(-\frac{t}{\rho\omega\sigma_{\rm sic}^2}\right). \tag{15}$$

Further, by substituting $f_T(t)$ and $f_S(s)$ into (14), and exploiting the integral tables in [22], (10) is obtained and the proof is completed. Similarly, the coverage region for user $u_{\rm t}$ can defined as

$$R_{\rm t}^{\mathcal{N}} \leq \mathbb{E}_{w_{\rm t}}\left[\log_2\left(1+\frac{\rho p_{\rm t}\beta_{\rm t}^2 d^{-\alpha}d_{\rm t}^{-\alpha}w_{\rm t}}{\rho p_{\rm r}\beta_{\rm t}^2 d^{-\alpha}d_{\rm t}^{-\alpha}w_{\rm t}+1}\right)\right] \tag{16}$$

$$= \int_0^{\infty}\log_2\left(1+\frac{\rho p_{\rm t}\beta_{\rm t}^2 d^{-\alpha}d_{\rm t}^{-\alpha}w_{\rm t}}{\rho p_{\rm r}\beta_{\rm t}^2 d^{-\alpha}d_{\rm t}^{-\alpha}w_{\rm t}+1}\right)f_{W_{\rm t}}(w_{\rm t})dw_{\rm t} \tag{17}$$

$$= \frac{1}{\Gamma(\kappa)\tau^{\kappa}}\int_0^{\infty}w_{\rm t}^{\kappa-1}{\rm e}^{-\frac{w_{\rm t}}{\tau}}\log_2\left(1+\frac{\rho p_{\rm t}\beta_{\rm t}^2 d^{-\alpha}d_{\rm t}^{-\alpha}w_{\rm t}}{\rho p_{\rm r}\beta_{\rm t}^2 d^{-\alpha}d_{\rm t}^{-\alpha}w_{\rm t}+1}\right)dw_{\rm t} \tag{18}$$

$$= \frac{1}{\Gamma(\kappa)\tau^{\kappa}\ln 2}\int_0^{\infty}w_{\rm t}^{\kappa-1}{\rm e}^{-\frac{w_{\rm t}}{\tau}}\ln\left(1+\frac{\rho\beta_{\rm t}^2 w_{\rm t}}{d^{\alpha}d_{\rm t}^{\alpha}}\right)dw_{\rm t} - \frac{1}{\Gamma(\kappa)\tau^{\kappa}\ln 2}\int_0^{\infty}w_{\rm t}^{\kappa-1}{\rm e}^{-\frac{w_{\rm t}}{\tau}}\ln\left(1+\frac{\rho p_{\rm r}\beta_{\rm t}^2 w_{\rm t}}{d^{\alpha}d_{\rm t}^{\alpha}}\right)dw_{\rm t}, \tag{19}$$

where, by assuming $q_{\rm t} = \frac{\rho\beta_{\rm t}^2}{d^{\alpha}d_{\rm t}^{\alpha}}w_{\rm t}$, $v_{\rm t} = \frac{\rho p_{\rm r}\beta_{\rm t}^2}{d^{\alpha}d_{\rm t}^{\alpha}}w_{\rm t}$, and using the Meijer's G-function instead of the logarithm [23], we have

$$R_{\rm t}^{\mathcal{N}} \leq \frac{1}{\Gamma(\kappa)\tau^{\kappa}\ln 2}\left(\frac{d^{\alpha}d_{\rm t}^{\alpha}}{\rho\beta_{\rm t}^2}\right)^{\kappa} \times \int_0^{\infty}q_{\rm t}^{\kappa-1}{\rm e}^{-\frac{d^{\alpha}d_{\rm t}^{\alpha}}{\rho\tau\beta_{\rm t}^2}q_{\rm t}}G_{2,2}^{1,2}\left(q_{\rm t}\,\middle|\,\begin{matrix}(1,1)\\(1,0)\end{matrix}\right)dq_{\rm t} - \frac{1}{\Gamma(\kappa)\tau^{\kappa}\ln 2}\left(\frac{d^{\alpha}d_{\rm t}^{\alpha}}{\rho p_{\rm r}\beta_{\rm t}^2}\right)^{\kappa} \times \int_0^{\infty}v_{\rm t}^{\kappa-1}{\rm e}^{-\frac{d^{\alpha}d_{\rm t}^{\alpha}}{\rho p_{\rm r}\tau\beta_{\rm t}^2}v_{\rm t}}G_{2,2}^{1,2}\left(v_{\rm t}\,\middle|\,\begin{matrix}(1,1)\\(1,0)\end{matrix}\right){\rm d}v_{\rm t}, \tag{20}$$

where the above integrals can be calculated with the help of [23, Eq. 2.24.3.1] and the proof is completed. ■

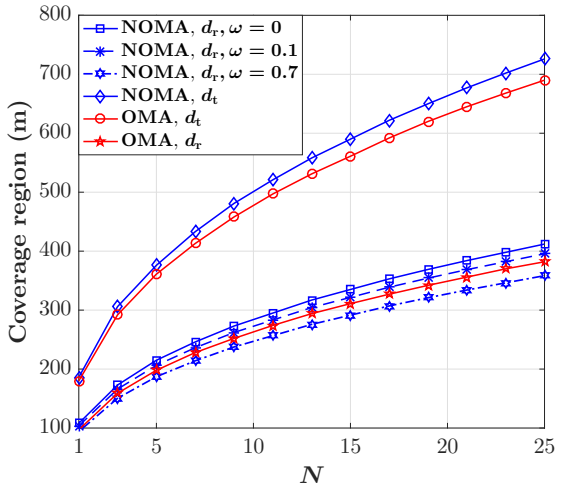

Fig. 2. The coverage regions d_r and d_t versus the number of STAR-RIS elements N.

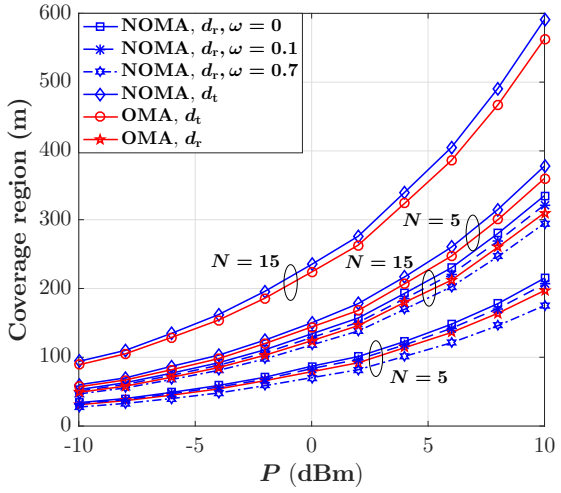

Fig. 3. The coverage regions d_r and d_t versus the transmit power P.

Theorem 2. *The coverage region over a STAR-RIS-aided OMA communication for the user u_k with defined parameters $R_k^{\mathcal{O}}$, κ, τ, and ρ is respectively given by*

$$R_k^{\mathcal{O}} \leq \frac{\delta_k}{\Gamma(\kappa)\ln 2} G_{3,2}^{1,3}\left(\frac{\tau\rho p_k \beta_k^2}{\delta_k d^\alpha d_k^\alpha} \middle| \begin{matrix} (1-\kappa,1,1) \\ (1,0) \end{matrix} \right). \quad (21)$$

Proof. Defining $\delta_k \in [0,1]$ as the share of resources allocated to each user in OMA [14], and under the same power constraint as in the NOMA case [24], we have

$$R_k^{\mathcal{O}} \leq \mathbb{E}_{w_k}\left[\delta_k \log_2\left(1 + \frac{\rho p_k \beta_k^2 w_k}{\delta_k d^\alpha d_k^\alpha}\right)\right]. \quad (22)$$

With these definitions, the proof is directly obtained following similar steps as those in the proof of Theorem 1. ■

IV. Numerical Results

We present numerical results to evaluate the analytical expressions previously derived. We assume that the BS is located at the origin of the two-dimensional coordinate and the STAR-RIS with N elements is placed $d = 800$ meters away from it. We also set $P = 10$dBm, $\sigma^2 = -114$dBm, $\sigma_{sic}^2 = -10$dB, $\beta_r = 0.8$, $\beta_t = 0.6$, $p_r = 0.4$, $p_t = 0.6$, $\alpha = 2.5$, $R_r^{\mathcal{K}} = 1$bps/Hz, and $R_t^{\mathcal{K}} = 0.3$bps/Hz for $\mathcal{K} \in \{\mathcal{N}, \mathcal{O}\}$. In addition, we consider the power allocation factor and the time allocation factor for both users in OMA as $p_k = 0.5$ and $\delta_k = 0.5$, respectively [7].

Fig. 2 shows the performance of the coverage region for both reflecting and transmitting users based on the number of STAR-RIS elements N and the controlling factor of the imperfect SIC ω. We see that as N increases, the STAR-RIS covers a larger area for users u_r and u_t. In addition, we can observe that user u_t can be located in a region further away from the STAR-RIS compared with user u_r, which confirms the adequacy of STAR-RIS to support outdoor users. Moreover, it is observed that the STAR-RIS under NOMA scenario

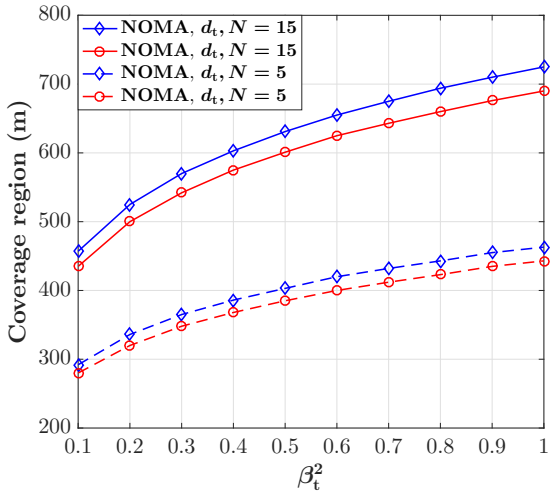

Fig. 4. The coverage region d_t versus the square of the transmission coefficient β_t^2.

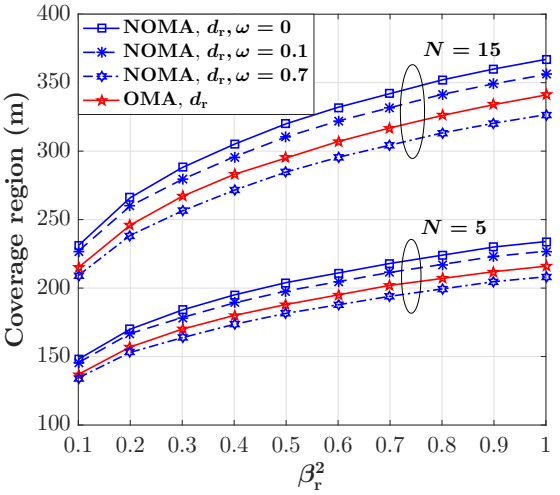

Fig. 5. The coverage region d_r versus the square of the reflection coefficient β_r^2.

provides a remarkable performance in terms of the coverage region compared with the OMA case since the simultaneously transmitting and reflecting scheme can increase the channel disparity between these two, where NOMA provides better performance than OMA. Furthermore, we can see that a larger coverage area for the user $u_{\rm r}$ is provided under perfect SIC scenario (i.e., $\omega = 0$) compared with the imperfect SIC cases for all considered values of N. The behavior of the coverage region for users $u_{\rm r}$ and $u_{\rm t}$ in terms of the transmit power P is presented in Fig. 3. In this figure, we observe that for a fixed value of P, increasing the number of STAR-RIS elements has a more noticeable effect on the variation of distance $d_{\rm t}$ compared with $d_{\rm r}$. It is also clear that under perfect SIC case, NOMA provides a larger coverage region for both users $u_{\rm t}$ and $u_{\rm r}$. This is also the case when assuming a residual imperfect SIC error (i.e., low ω). However, as ω increases, the OMA scenario can even outperform the NOMA case in terms of the coverage region for user $u_{\rm r}$. It can be seen from Thms. 1 and 2 that the coverage region for each user highly depends on its corresponding reflection/transmission coefficients. In this regard, Figs. 4 and 5 show the coverage regions $d_{\rm t}$ and $d_{\rm r}$ in terms of the square of the reflection and transmission coefficients $\beta_{\rm t}^2$ and $\beta_{\rm r}^2$, respectively. In both figures, it is observed that as $\beta_{\rm k}^2$ grows, a larger coverage area can be provided by the STAR-RIS for the respective user $u_{\rm k}$. In addition, by comparing these two figures, we can see that under an equal value of reflection and transmission coefficients (i.e., $\beta_{\rm r}^2 = \beta_{\rm t}^2 = 0.5$), STAR-RIS offers a larger coverage area for user $u_{\rm t}$. The aforesaid results indicate that applying the STAR-RIS into NOMA networks under perfect and moderately imperfect SIC improves the system performance in terms of the coverage region.

V. Conclusion

In this paper, we analyzed a downlink STAR-RIS-aided NOMA/OMA communication system, and provided analytical expressions for the coverage regions for users in the transmission and reflection planes of the STAR-RIS under the energy-splitting protocol. By considering the imperfect SIC, we showed that the use of STAR-RIS provides a larger coverage area for *both* transmitting and reflecting users in the NOMA network compared to the benchmark OMA system.

References

[1] E. Basar, M. Di Renzo, J. De Rosny, M. Debbah, M.-S. Alouini, and R. Zhang, "Wireless communications through reconfigurable intelligent surfaces," *IEEE Access*, vol. 7, pp. 116 753–116 773, 2019.

[2] S. Basharat, S. A. Hassan, H. Pervaiz, A. Mahmood, Z. Ding, and M. Gidlund, "Reconfigurable intelligent surfaces: Potentials, applications, and challenges for 6G wireless networks," *IEEE Wireless Commun.*, vol. 28, no. 6, pp. 184–191, 2021.

[3] Q. Wu, S. Zhang, B. Zheng, C. You, and R. Zhang, "Intelligent reflecting surface-aided wireless communications: A tutorial," *IEEE Trans. Commun.*, vol. 69, no. 5, pp. 3313–3351, 2021.

[4] Y. Liu, X. Mu, J. Xu, R. Schober, Y. Hao, H. V. Poor, and L. Hanzo, "STAR: Simultaneous transmission and reflection for 360 coverage by intelligent surfaces," *IEEE Wireless Commun.*, vol. 28, no. 6, pp. 102–109, 2021.

[5] H. Zhang, S. Zeng, B. Di, Y. Tan, M. Di Renzo, M. Debbah, Z. Han, H. V. Poor, and L. Song, "Intelligent omni-surfaces for full-dimensional wireless communications: Principles, technology, and implementation," *IEEE Commun. Mag.*, vol. 60, no. 2, pp. 39–45, 2022.

[6] X. Mu, Y. Liu, L. Guo, J. Lin, and R. Schober, "Simultaneously transmitting and reflecting (STAR) RIS aided wireless communications," *IEEE Trans. Wireless Commun.*, vol. 21, no. 5, pp. 3083–3098, 2021.

[7] C. Wu, X. Mu, Y. Liu, X. Gu, and X. Wang, "Resource allocation in STAR-RIS-aided networks: OMA and NOMA," *IEEE Trans. Wireless Commun.*, vol. 21, no. 9, pp. 7653–7667, 2022.

[8] A. Palomares-Caballero, C. Molero Jiménez, F. R. Ghadi, F. J. López-Martínez, P. Padilla, D. Morales-Jimenez, and J. Valenzuela-Valdés, "Enabling Intelligent Omni-Surfaces in the Polarization Domain: Principles, Implementation and Applications," *IEEE Commun. Mag.*, in press 2023.

[9] C. Wu, C. You, Y. Liu, X. Gu, and Y. Cai, "Channel estimation for STAR-RIS-aided wireless communication," *IEEE Commun. Lett.*, vol. 26, no. 3, pp. 652–656, 2021.

[10] M. Aldababsa, A. Khaleel, and E. Basar, "Simultaneous transmitting and Reflecting Intelligent surfaces-empowered NOMA networks," *arXiv preprint arXiv:2110.05311*, 2021.

[11] C. Zhang, W. Yi, Y. Liu, Z. Ding, and L. Song, "STAR-IOS aided NOMA networks: Channel model approximation and performance analysis," *IEEE Trans. Wireless Commun.*, vol. 21, no. 9, pp. 6861–6876, 2022.

[12] X. Yue, J. Xie, Y. Liu, Z. Han, R. Liu, and Z. Ding, "Simultaneously transmitting and reflecting reconfigurable intelligent surface assisted NOMA networks," *IEEE Trans. Wireless Commun.*, vol. 22, no. 1, pp. 189–204, 2022.

[13] T. Wang, M.-A. Badiu, G. Chen, and J. P. Coon, "Outage probability analysis of STAR-RIS assisted NOMA network with correlated channels," *IEEE Commun. Lett.*, vol. 26, no. 8, pp. 1774–1778, 2022.

[14] C. Wu, Y. Liu, X. Mu, X. Gu, and O. A. Dobre, "Coverage characterization of STAR-RIS networks: NOMA and OMA," *IEEE Commun. Lett.*, vol. 25, no. 9, pp. 3036–3040, 2021.

[15] V. Aggarwal, A. Bennatan, and A. R. Calderbank, "On maximizing coverage in Gaussian relay channels," *IEEE Trans. Inf. Theory*, vol. 55, no. 6, pp. 2518–2536, 2009.

[16] Z. Chen, Z. Ding, X. Dai, and G. K. Karagiannidis, "On the application of quasi-degradation to MISO-NOMA downlink," *IEEE Trans. Signal Process.*, vol. 64, no. 23, pp. 6174–6189, 2016.

[17] J. Zhu, Y. Huang, J. Wang, K. Navaie, and Z. Ding, "Power efficient IRS-assisted NOMA," *IEEE Trans. Commun.*, vol. 69, no. 2, pp. 900–913, 2020.

[18] C.-L. Wang, C.-C. Hsieh, Y.-C. Ding, and S.-H. Huang, "Power allocation for downlink NOMA systems with imperfect channel estimation," in *2021 IEEE Wireless Communications and Networking Conference (WCNC)*, 2021, pp. 1–7.

[19] Z. Chen, Z. Ding, X. Dai, and R. Zhang, "An optimization perspective of the superiority of NOMA compared to conventional OMA," *IEEE Trans. Signal Process.*, vol. 65, no. 19, pp. 5191–5202, 2017.

[20] S. Atapattu, R. Fan, P. Dharmawansa, G. Wang, J. Evans, and T. A. Tsiftsis, "Reconfigurable intelligent surface assisted two–way communications: Performance analysis and optimization," *IEEE Trans. Commun.*, vol. 68, no. 10, pp. 6552–6567, 2020.

[21] A. Lozano and N. Jindal, "Are yesterday's information-theoretic fading models and performance metrics adequate for the analysis of today's wireless systems?" *IEEE Commun. Mag.*, vol. 50, no. 11, pp. 210–217, 2012.

[22] D. Zwillinger and A. Jeffrey, *Table of integrals, series, and products*. Elsevier, 2007.

[23] A. Prudnikov, Y. A. Brychkov, and O. Marichev, "More special functions (integrals and series vol 3)," 1990.

[24] Z. Chen, Z. Ding, X. Dai, and R. Zhang, "An optimization perspective of the superiority of noma compared to conventional oma," *IEEE Trans. Signal Process.*, vol. 65, no. 19, pp. 5191–5202, 2017.